AFRL-SR-AR-TR-03-

0127

REPORT DOCUMENTATION PAGE

1. REPORT DATE (DD-MM-YYYY)	2. REPORT TYPE	3. DATES COVERED (From - To)
31 08 2001	Annual Performance & Final	01 12 2000 - 25 08 2001

4. TITLE AND SUBTITLE

~~Experimental and Theoretical Studies of NCl Kinetics~~

5a. CONTRACT NUMBER

5b. GRANT NUMBER

F49620-01-1-~~0700~~ 0070

5c. PROGRAM ELEMENT NUMBER

6. AUTHOR(S)

Michael C. Heaven

5d. PROJECT NUMBER

5e. TASK NUMBER

5f. WORK UNIT NUMBER

7. PERFORMING ORGANIZATION NAME(S) AND ADDRESS(ES)

Emory University
1784 N. Decatur Road
Suite 510
Atlanta, GA 30322

8. PERFORMING ORGANIZATION REPORT NUMBER

9. SPONSORING / MONITORING AGENCY NAME(S) AND ADDRESS(ES)

AFOSR
801 N. Randolph Street
Suite 732
Arlington, VA 22203-1977

10. SPONSOR/MONITOR'S ACRONYM(S)

11. SPONSOR/MONITOR'S REPORT NUMBER(S)

12. DISTRIBUTION / AVAILABILITY STATEMENT

Unlimited / Unclassified

13. SUPPLEMENTARY NOTES

14. ABSTRACT NCl(a) is the energy carrier in the all gas phase iodine laser (AGIL). Studies of NCl(a,X) kinetics are being performed using photolysis of ClN_3 as the source of the radical. Photodissociation of ClN_3 is being characterized using photoionization mass spectrometry and time-resoled IR emission spectroscopy. The fluorescence quantum yield for NCl(a) has been estimated, and the products Cl+N_3 detected.

Theoretical studies of NCl+NCl reactions are in progress. For NCl(a)+NCl(a) the potential energy surface intersections responsible for the energy pooling process NCl(a)+NCl(a) $\rightarrow$NCl(b)+NCl(X) have been located. These intersections lie just above the entrance channel, and are accessible to thermal collisions. It is confirmed that rapid self-removal of NCl(X) ($k=8\times10^{-12}$ cm^3 s^{-1}) proceeds via the reaction NCl(X)+NCl(X) $\rightarrow N_2$+2Cl.

Potential energy surfaces for the reaction Cl+$N_3\rightarrow$NCl+N_2 have been calculated. A barrier 16.6 kcal/mol barrier was located on the triplet surface, which accounts for the preference for singlet products. Branching ratio calculations are in progress.

The reactions H+$X_2\rightarrow$HX+X (X=F, Cl) are of importance in HX chemical lasers. The uncertainties associated with the rate constants are too large for accurate computational modeling of laser systems. These constants are being re-measured using photolysis/LIF probe techniques.

15. SUBJECT TERMS

Chemical Lasers, AGIL, Iodine laser, HF laser, Energy transfer.

16. SECURITY CLASSIFICATION OF:			17. LIMITATION OF ABSTRACT	18. NUMBER OF PAGES	19a. NAME OF RESPONSIBLE PERSON
a. REPORT	b. ABSTRACT	c. THIS PAGE			Michael C. Heaven
Unclassified	Unclassified	Unclassified	Unlimited	20	19b. TELEPHONE NUMBER (include area code) (404) 727 6617

Energy Transfer Kinetics and Dynamics of Relevance to Iodine Lasers.

Progress Report for December 1, 2000 to August 25, 2001

Grant #: AFOSR F49620-01-1-0070

Work performed at the Department of Chemistry, Emory University, Atlanta, GA 30322.

Personnel:

Michael C. Heaven (P.I.)

Keiji Morokuma (Senior collaborator)

Alexey L. Kaledin (fith year graduate student, jointly supervised by the P.I. and Prof. K. Morokuma)

Anatoly V. Komissarov (fourth year graduate student)

Summary of Progress and Results

1. Photodissociation dynamics of ClN_3

Photolysis of ClN_3 is a useful source of NCl(a) for kinetic measurements. For experiments conducted under pseudo fist order conditions it is sufficient to know the relative concentration of NCl(a), but the absolute value is not needed. However, to determine rate constants under second order conditions knowledge of the absolute concentration of NCl(a) is needed. One of the goals of this research has been measurement of the second order rate constant for self-annihilation of NCl(a). The technique we have applied to generate known quantities of NCl(a) involves complete photodissociation of a known concentration of ClN_3. This can yield well-defined quantities of NCl(a) provided that the branching fraction for this product is known. It is established that NCl(a) is the dominant product, but NCl(b) and NCl(X) are also produced. In addition, the channel $ClN_3+hv \rightarrow Cl+N_3$ is open. Previously we had used dispersed fluorescence to observe singlet NCl and absorption measurements to monitor NCl(X). The limitations of this approach were that we could not verify total destruction of ClN_3 by direct observation, and that non-fluorescing products (other than NCl(X)) could not be monitored. To improve our knowledge of ClN_3 photodissociation dynamics we examined the potential for using photo-ionization mass spectrometry as a more versatile detection method. We began these studies by using pulsed 118 nm light to ionize ClN_3. To generate VUV pulses we added a frequency-tripling cell to our TOF mass spectrometer, which was used to up

convert the third harmonic from an Nd/YAG laser. Fig. 1 shows the mass spectrum obtained using 118 nm pulses to excite ClN_3. Surprisingly, the azide did not survive this rather gentle method of

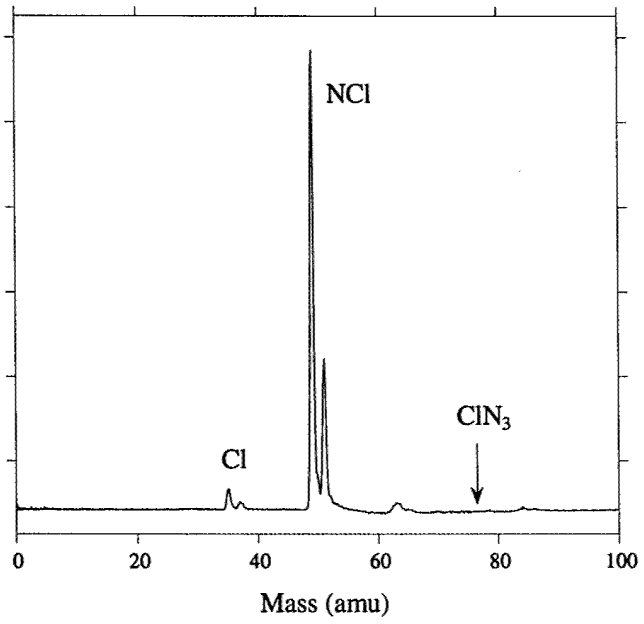

Figure 1. Mass spectrum obtained by 118 nm excitation of ClN_3

ionization. The position where the ClN_3 should appear is indicated in Fig. 1, but there was no discernable signal at this mass. It appears that 118 nm light causes a dissociative ionization of ClN_3 of the type

$$ClN_3 + h\nu(118\ nm) \rightarrow NCl^+ + N_2.$$

Hence this approach is not suitable for monitoring ClN_3 in experiments where alternative pathways for generating NCl exist. We also examined the possibility of using excimer laser pulses (193 or 248 nm) to effect multi-photon ionization of ClN_3. The results of these experiments are shown in Figs 2 and 3. Note that the excimer laser pulses fragmented and ionized the background pump oil in the mass spectrometer chamber (evacuated to $2x10^{-7}$ Torr). The downward-going traces of Figs 2 and 3 show the background spectra, which consisted mostly of hydrocarbon fragments. The upward-going traces were taken with ClN_3 present. Neither of the photoexcitation wavelengths generated detectable

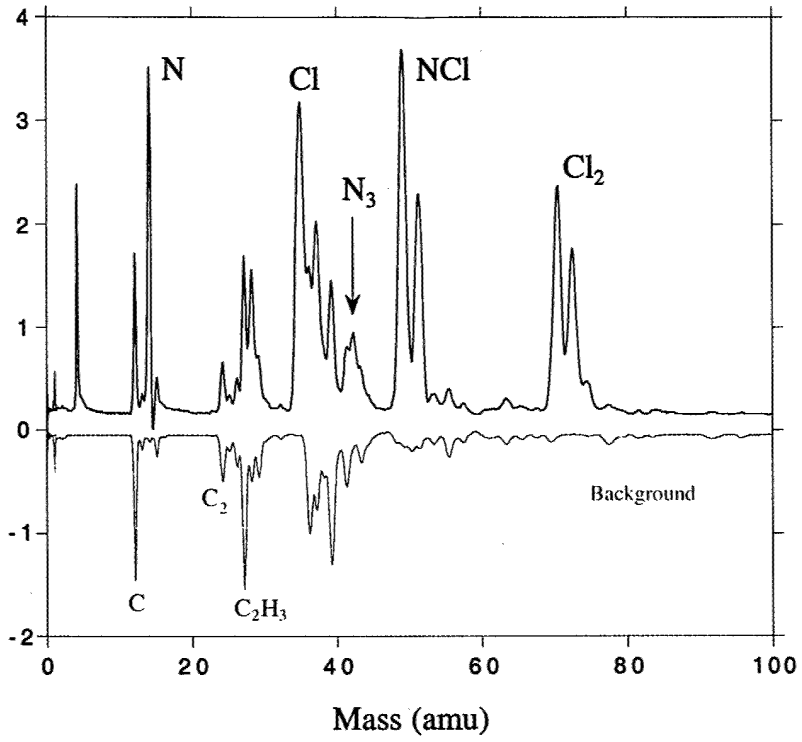

Figure 2. Mass spectrum obtained by multiphoton excitation of ClN_3 at 193 nm

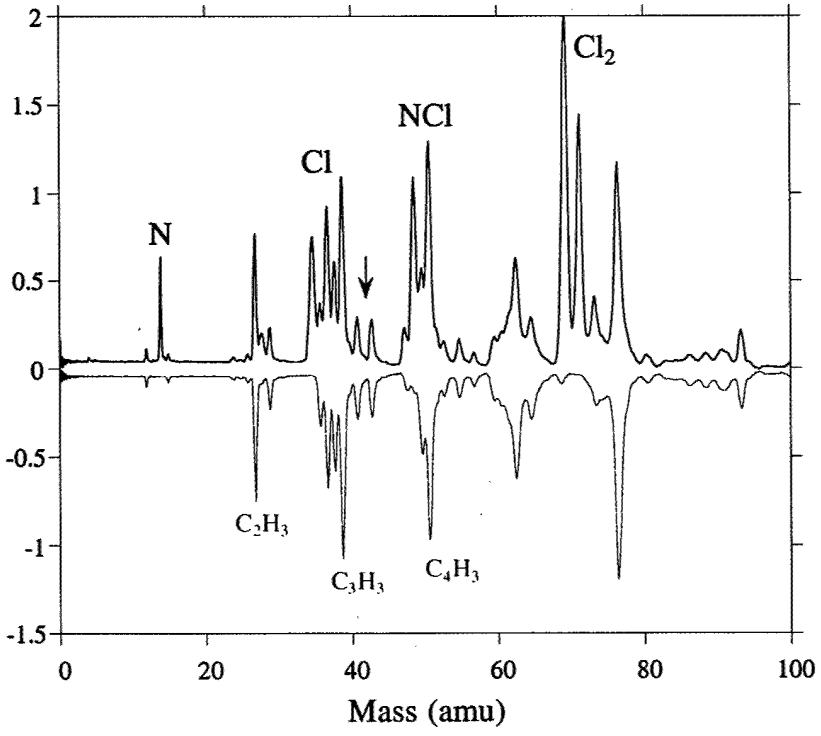

Figure 3. Mass spectrum obtained by multiphoton excitation of ClN_3 at 248 nm

quantities of ClN_3^+. Again, fragmentation to produce NCl^+ dominated the kinetics. Note that excitation at 193 nm produced N_3^+, which suggests the possible production sequence

$$ClN_3 + h\nu \rightarrow Cl + N_3$$

$$N_3 + 2h\nu \rightarrow N_3^+$$

Evidence that 193 nm light can cause the first step was obtained in a study of the IR emission (see below). The arrow in Fig. 3 marks the position where N_3 should be observed in the mass spectrum recorded using 248 nm light. The absence of N_3 in this spectrum may indicate that the path to $Cl+N_3$ represents a very minor channel for 248 nm photolysis.

In previous studies we examined the kinetics of NCl(X) production when ClN_3/O_2 mixtures were photolyzed. The purpose of these measurements was to determine the branching fraction for formation of NCl(a). As the experiments involved monitoring a single ro-vibrational level of NCl(X) v=0, the role of ro-vibrational relaxation in the observed kinetics was an open question. Initial kinetic models required the assumption that UV photolysis of ClN_3 yielded NCl(X) $v\geq1$ with a branching fraction of about 20%. However, attempts to detect population in the v=1 and 2 states by transient absorption were unsuccessful. As an alternative means for characterizing these products we attempted to detect IR fluorescence from NCl following photolysis of ClN_3. These experiments were conducted in collaboration with Prof. Hai-Lung Dai at the University of Pennsylvania. The apparatus used is shown in Fig. 4. ClN_3 was photolyzed by 193 nm pulses from an excimer laser. The frequency and temporal characteristics of the resulting IR fluorescence were recorded using a time-resolved FTIR spectrometer. Fig. 5 shows a typical emission spectrum. The only significant feature in this trace is the emission from N_3 (asymmetric stretch fundamental) at 1644 cm^{-1}. There was no sign of IR emission from NCl(X). Unfortunately, the absence of NCl(X) bands is not conclusive evidence that this product is vibrationally cold. The transition dipole for NCl(X) IR emission is rather small, and occurs near the long wavelength cut-off of the HgCdTe detector. Conversely, the transition dipole for the asymmetric stretch of N_3 is relatively large, and the emission occurs in a spectral range that is better suited for the detector. Hence, although we could observe N_3 this does not necessarily indicate that dissociation to give $Cl+N_3$ is a dominant channel. By comparison with isovalent HN_3 we estimate that about 15% of the 193 nm photolysis events give $Cl+N_3$.

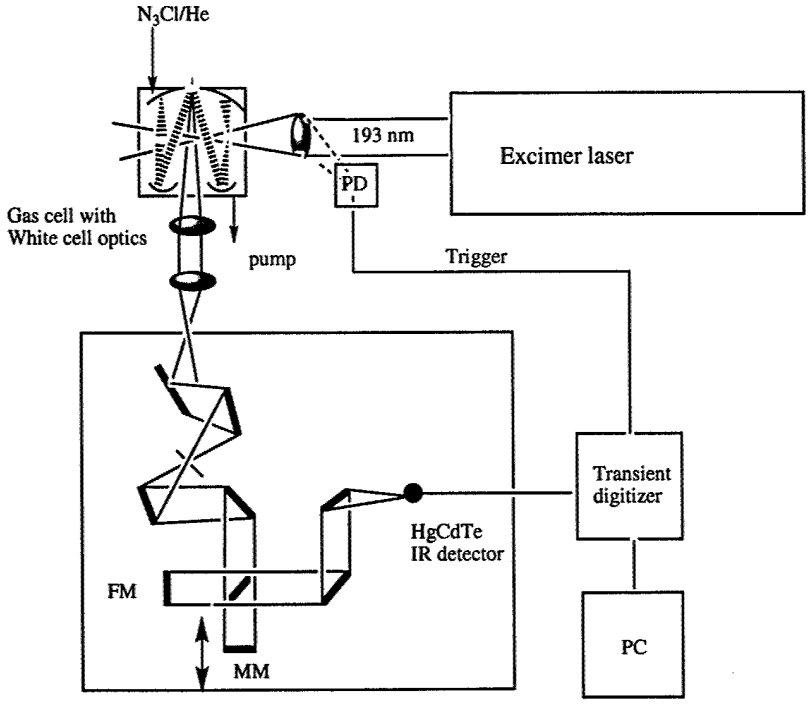

Figure 4. Apparatus used for time-resolved FTIR study of ClN_3 photolysis

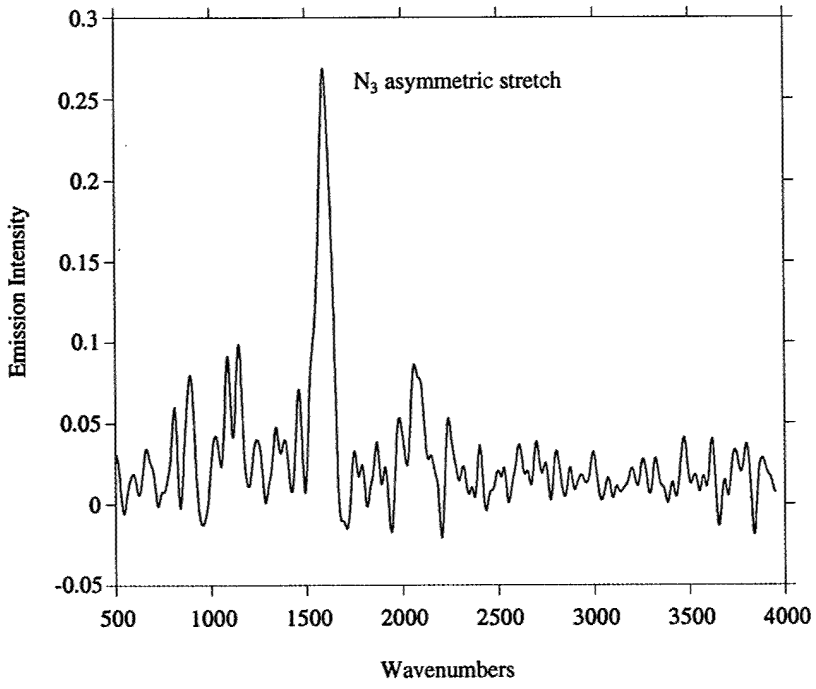

Figure 5. IR emission from photolysis of ClN_3 at 193 nm.

Different electronic transitions of ClN_3 are accessed by 193 and 248 nm excitation. A similar situation exists for HN_3, where the maxima of the two systems are shifted to longer wavelengths. Photolysis of HN_3 via the lower energy state (e.g., 266 nm excitation) gives a small yield of $H+N_3$ (4%), whereas excitation to the higher energy state (248 nm excitation) yields 20% $H+N_3$. The data from our mass spectrometry experiments suggest that ClN_3 behaves similarly, and that the yield of $Cl+N_3$ from 248 nm photolysis (excitation to the lower energy state) will be small.

In future investigations of the IR emissions we plan to examine 248 nm photolysis and use detectors that are better suited for 800-1000 cm^{-1} radiation.

Combining a conservative estimate of 15% for the 248 nm yield of $Cl+N_3$ with the NCl(a) branching fraction from the NCl(X) absorption measurements ($[NCl(a)]_0/([NCl(a)]_0+[NCl(X)]_0)\geq 0.9$) we obtain a quantum yield for formation of NCl(a) of 76%. This value, applied to the data from our previous NCl(a) self-removal study, yields a second order rate constant of 6.2×10^{-13} cm^3 s^{-1}. Henshaw et al. reported a self-annihilation rate constant that was more than an order of magnitude greater than this value ($(7.2\pm0.9)\times10^{-12}$ cm^3 s^{-1}). For our fluorescence decay data to be consistent with this value the quantum yield for NCl(a) formation would have to be just 7%. This is unreasonably low. All other estimates for the quantum yield exceed 50%. The demonstration of I* lasing via photolysis of ClN_3/CH_2I_2 mixtures further attests to the high quantum yield.

2. Construction of a heated photolysis cell

In the original proposal we had planned to study the temperature dependencies of the NCl(a) quenching rate constants and the self-annihilation reaction using a heated flow tube with mass spectrometric detection. We have since discovered complications with this approach that are associated with the dissociative photoionization of ClN_3, and developed a technique for characterizing the self-annihilation process using fluorescence detection. Consequently, we are now constructing a heated photolysis cell that is configured for fluorescence detection. This apparatus will be used to explore the temperature dependence of NCl(a)+M, where M=NCl(a), HF, HCl, HI, Cl_2, and ClN_3. Recent model calculations (P. Crowel, Logicon RDA) indicate that the Cl atoms released by the reaction

$$NCl(X) + NCl(X) \rightarrow N_2 + 2Cl \qquad (1)$$

may pose a serious problem in the NCl/I laser as Cl is an efficient quencher of I*. At present the temperature dependence of the I*+Cl quenching rate constant is not known. The heated photolysis cell will be used to obtain this information.

3. Theoretical studies of NCl + NCl interactions.

To gain deeper insights concerning the self-annihilation of NCl(a) and the range of possible products from NCl(X) + NCl(X) we have examined NCl – NCl interactions using high-level theoretical methods. This work is being carried out in collaboration with Prof. Keiji Morokuma and Dr. Gregory S. Tschumper at Emory.

One of the issues explored in this study was the stability of ground state N_2Cl_2. Recent BP86 density functional calculations had indicated that both the *cis-* and *trans-* isomers were stable, with the former being a little more deeply bound. We applied a number of multi-reference techniques in our calculations. The active spaces used for these calculations can be defined in terms of the natural orbitals depicted in Fig. 6 (for the *trans-* isomer). The 6 electron 6 orbital (6x6), and 8 electron, 8 orbital (8x8) spaces are indicated. A few full valence calculations (24x16) were also carried out. The 6-311+G(d) basis set was used with the CASSCF and CAPT2 methods. In addition, coupled cluster calculations (CCSD(T)) were performed with the TZ2P and TZ2P(f) basis sets. Results from these calculations for the *cis-* and *trans-*isomers are presented in Fig. 7 and Table 1. Here we use the notation $N_2Cl_2^{\dagger}$ to designate the saddle point that separates N_2Cl_2 from N_2+2Cl. Regardless of the size of the active space, CASSCF predicts that N_2Cl_2 is unstable with respect to dissociation to N_2+2Cl. It appears that the previous predictions of stable structures were an artifact resulting from the use of a single reference approximation. CASPT2 and CCSD(T) calculations predict very shallow minima for the *cis-* and *trans-* structures. The exact locations of the CASPT2 saddle points were not determined. The CCSD(T)/TZ2P(f) saddle points yield barriers to dissociation of 8.0 kcal/mol (*trans*) and 7.3 kcal /mol (*cis*). These barriers are not high enough to make N_2Cl_2 a stable species. This is consistent with the fact that there have been no experimental observations of this molecule.

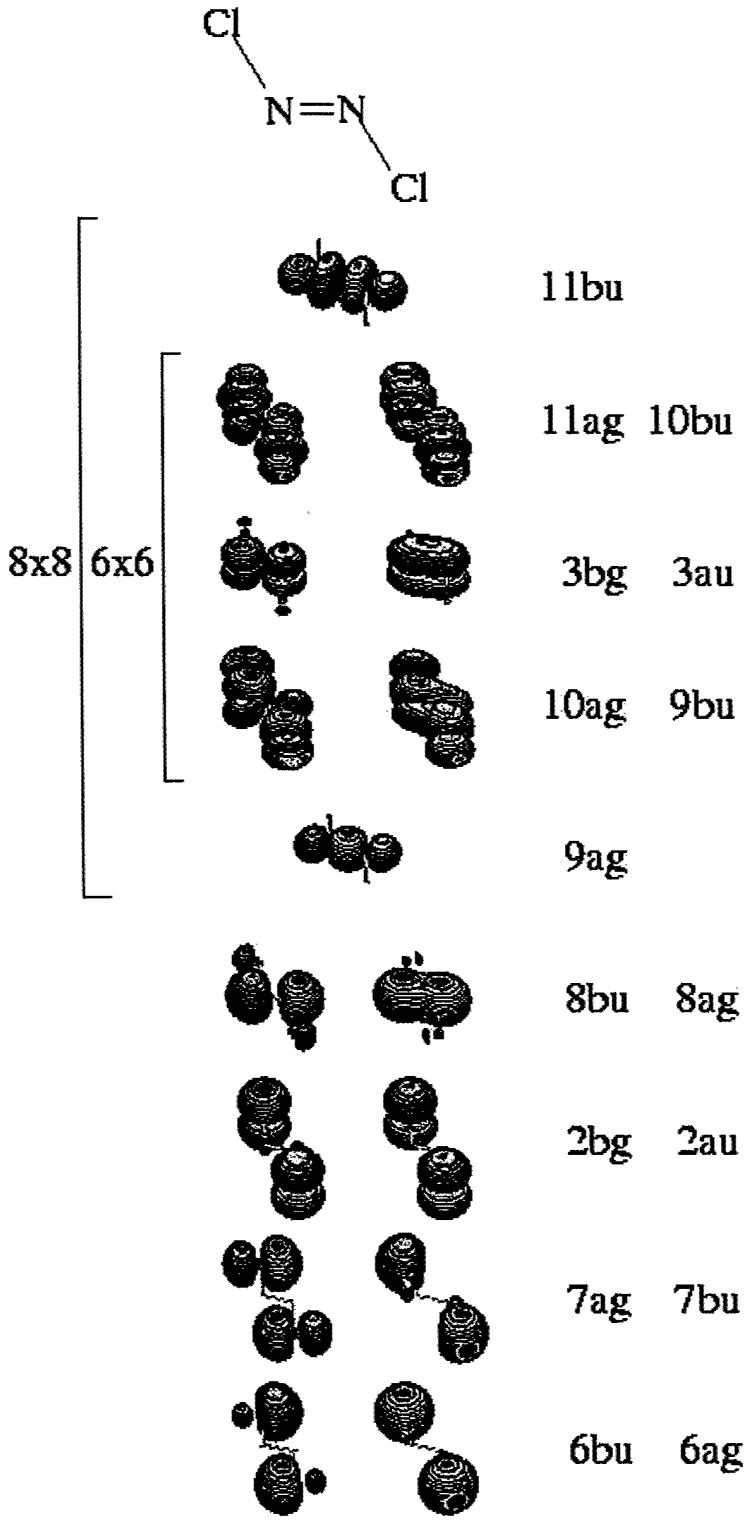

Figure 6. Natural orbitals for *trans*- ClN-NCl

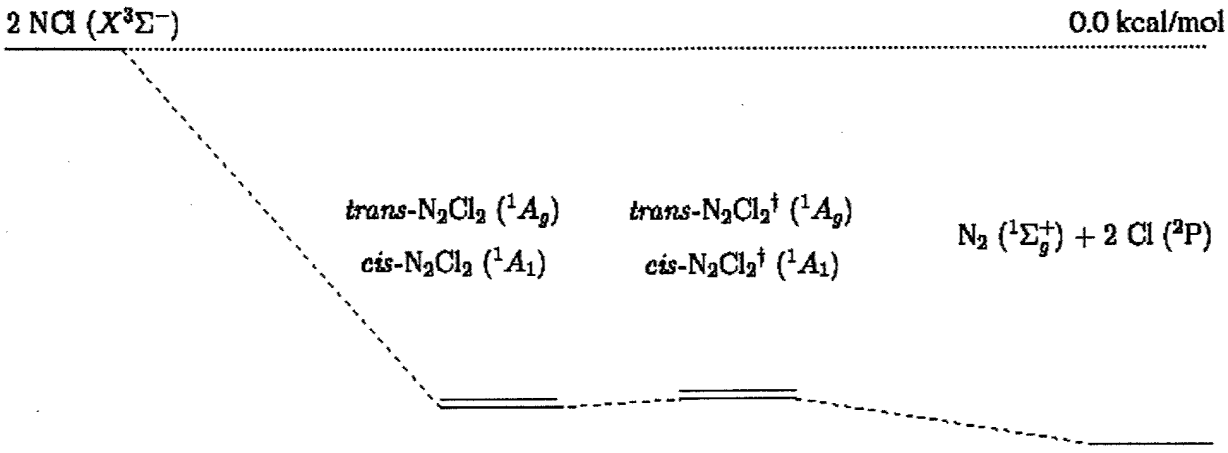

Energies (in kcal/mol) of key stationary points relative to the NCl ($X^3\Sigma^-$) + NCl ($X^3\Sigma^-$) assymptote.

Method	Basis	*trans*-N_2Cl_2	*cis*-N_2Cl_2	*trans*-$N_2Cl_2^\dagger$	*cis*-$N_2Cl_2^\dagger$	N_2+ 2 Cl
6 × 6 CASSCF	6-311+G(*d*)	minima and transition states do not exist				-116.2
8 × 8 CASSCF	6-311+G(*d*)	minima and transition states do not exist				...
24 × 16 CASSCF	6-311+G(*d*)	minima and transition states do not exist				-137.9
6 × 6 CASPT2	6-311+G(*d*)	-82.4	-84.4	...	...	...
8 × 8 CASPT2	6-311+G(*d*)	-83.2	-86.5	...	...	...
CCSD(T)	TZ2P	-86.5	-92.9	-82.0	-87.0	-106.1
CCSD(T)	TZ2P(*f*)	-88.6	-92.6	-80.6	-85.3	-102.3

Figure 7

Considering only the first three bound electronic states of NCl ($X^3\Sigma^-$, $a^1\Delta$ and $b^1\Sigma^+$), the interaction of two NCl molecules yields 18 electronic states. A one-dimensional cut through the ClN-NCl potential energy surfaces of the lower energy states is shown in Fig. 8. This plot corresponds to a rigid C_{2h} geometry, with variation of just the N-N distance. An interesting feature of Fig. 8 is the crossings between the lowest states of the $a^1\Delta$+$a^1\Delta$ with states from $X^3\Sigma$+$b^1\Sigma$ that occur near 2.4 Å. These crossings persist for many other geometries, and they occur at energies (relative to the $a^1\Delta$+$a^1\Delta$ asymptote) that are accessible to room temperature collisions. Table 2 lists the energies and geometries of the curve crossing for the *cis*- and *trans*-isomers.

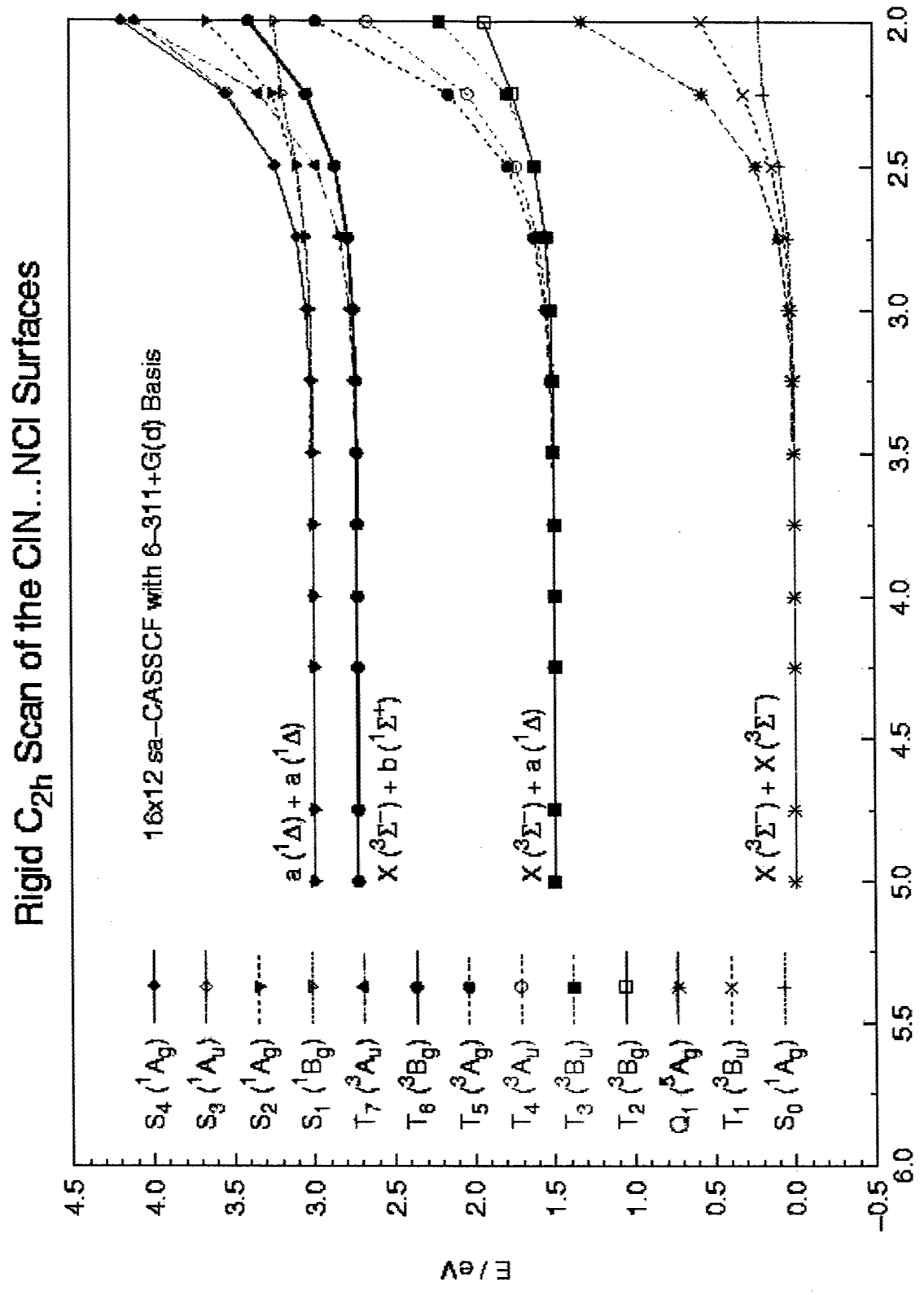
Rigid C_{2h} Scan of the ClN...NCl Surfaces
16x12 sa–CASSCF with 6–311+G(d) Basis
S_4 (^1A_g)
S_3 (^1A_u)
S_2 (^1A_g)
S_1 (^1B_g)
T_7 (^3A_u)
T_6 (^3B_g)
T_5 (^3A_g)
T_4 (^3A_u)
T_3 (^3B_u)
T_2 (^3B_g)
Q_1 (^5A_g)
T_1 (^3B_u)
S_0 (^1A_g)
a ($^1\Delta$) + a ($^1\Delta$)
X ($^3\Sigma^-$) + b ($^1\Sigma^+$)
X ($^3\Sigma^-$) + a ($^1\Delta$)
X ($^3\Sigma^-$) + X ($^3\Sigma^-$)
E / eV
NN distance / Angstroms
4.5
4.0
3.5
3.0
2.5
2.0
1.5
1.0
0.5
0.0
−0.5
6.0
5.5
5.0
4.5
4.0
3.5
3.0
2.5
2.0

Figure 8

Table 1

Optimized geometrical parameters (in Å and degrees) of key stationary points on the NCl ($X^3\Sigma^-$) + NCl ($X^3\Sigma^-$) surface.

Method	Basis	R(NN)	R(NCl)	θ(NNCl)
		Isolated N_2 and NCl		
6 × 6 CASPT2	6-311+G(d)	...	1.626	...
8 × 8 CASPT2	6-311+G(d)	...	1.639	...
R/ROCCSD(T)	TZ2P	1.103	1.665	...
R/ROCCSD(T)	TZ2P(f)	1.104	1.640	...
		cisN_2Cl_2		
6 × 6 CASPT2	6-311+G(d)	1.206	1.800	122.6
8 × 8 CASPT2	6-311+G(d)	1.208	1.803	122.6
RCCSD(T)	TZ2P	1.201	1.828	121.9
RCCSD(T)	TZ2P(f)	1.209	1.793	121.4
		transN_2Cl_2		
6 × 6 CASPT2	6-311+G(d)	1.223	1.802	108.4
8 × 8 CASPT2	6-311+G(d)	1.224	1.807	108.2
RCCSD(T)	TZ2P	1.221	1.819	107.4
RCCSD(T)	TZ2P(f)	1.227	1.786	107.8
		cisN_2Cl_2[†]		
6 × 6 CASPT2	6-311+G(d)	...	...	...
8 × 8 CASPT2	6-311+G(d)	...	...	...
RCCSD(T)	TZ2P	1.142	2.082	124.8
RCCSD(T)	TZ2P(f)	1.137	2.115	125.1
		transN_2Cl_2[†]		
6 × 6 CASPT2	6-311+G(d)	...	...	...
8 × 8 CASPT2	6-311+G(d)	...	...	...
RCCSD(T)	TZ2P	1.157	2.086	105.2
RCCSD(T)	TZ2P(f)	1.150	2.115	105.8

Table 2

Optimized geometrical parameters (in Å and degrees) and relative energies (in kcal mol^{-1}/mol) of some long range MSXs on the $a + a$ surface. The energies of the MSXs are relative to the NCl $(a^1\Delta) + $ NCl $(a^1\Delta)$ asymptotes. All values were obtained using the 16 × 12 state-averaged conjunctions with the 6-311+G(d) basis set.

$X + b$	$a + a$	R(NN)	R(NCl)	θ(NNCl)	ΔE_{MSX}
		cis-Conformation			
T7 ($^3B_1$)	S1 ($^1A_2$)	2.375	1.654	114.3	3.5
T7 ($^3B_1$)	S2 ($^1A_1$)	2.351	1.652	114.4	4.3
		trans-Conformation			
T7 (^3A_u)	S1 (^1A_g)	2.345	1.643	109.2	3.2
T7 (^3A_u)	S2 (^1B_g)	2.375	1.645	109.7	2.2

It is probable that these crossings are responsible for the energy pooling process

$$NCl(a)+NCl(a) \rightarrow NCl(b)+NCl(X)$$

Based on our NCl(a) self-annihilation rate constant and the rate constant for reaction 2 reported by Manke and Setser, the pooling reaction accounts for approximately 25% of the self removal process.

The calculations performed so far support the notion that reaction 1 rapidly removes NCl(X) and they indicate that electronic energy transfer via curve crossings contributes significantly to the self-removal of NCl(a). However, further test are needed to ensure that we have adequately converged results. Selected calculations that use full-valence, state averaged MCSCF will be used to test the reliability of the lower level methods.

5. Theoretical studies of the $Cl+N_3 \rightarrow NCl + N_2$ reaction.

The reaction $Cl + N_3 \rightarrow NCl + N_2$ is known to give substantial yields of NCl(*a*). The potential use of this reaction in a chemically driven iodine laser system is currently being evaluated. The branching ratio for $Cl + N_3 \rightarrow N_2 + NCl(a, b)$ (singlet product) vs. $Cl + N_3 \rightarrow N_2 + NCl(X)$ (triplet product) is a critical issue for laser pumping applications. In recent kinetic studies it has been determined that NCl(*a*) is formed with a yield in excess of 60%. However, it is a difficult matter to make a direct experimental determination of the branching ratio. To address this issue we are performing *ab initio* calculations to examine the singlet/triplet branching ratio from a theoretical perspective. This work is being done in collaboration with Prof. Keiji Morokuma and Mr. Graham Phillips.

Previously we examined qualitative features of the Cl-N_3 potential energy surfaces using the B3LYP/6-31+G(*d*) level of theory. Improved energies for the stationary points were then computed using CASSCF (12 electrons, 10 orbitals) followed by CASPT2 (8 electrons, 6 orbitals). The basis set used was of valence triple zeta quality (*spdf, sp+*). A puzzling feature of the results from these calculations was the low barrier (below the asymptotic reactant energy) for the reaction on the triplet surface ($Cl+N_3 \rightarrow NCl(X) + N_2$). With such a low barrier it was difficult to account for the observed preference for the formation of singlet products. We have now investigated this system using better quality basis functions. Our ability to perform such large calculations was greatly improved by upgrades in the Emerson Center computing facilities that were implemented at the beginning of this year. New maps of potential surfaces were constructed using B3LYP with the D95+*d* basis. Stationary points and minimum energy crossing points were optimized using CASSCF (12e/10o) with the D95+*d* basis. Results from the CASSCF calculations are summarized in Fig. 9. They are dramatically different from the results obtained with the 6-31+G(*d*) basis. We now find that the barrier to reaction on the triplet surface lies appreciably above the entrance channel, while the barrier to reaction on the singlet surface lies below the energy of the reactants. This readily explains the observed preference for the singlet products. Note that a seam of intersection exists between the singlet and triplet surfaces, and the minimum of this seam is indicated by the point S0T1TX in Fig. 9. This intersection occurs before the barrier on the singlet surface, and may well influence the singlet/triplet product branching ratios.

Next we will carry out dynamical studies using the potential energy surfaces to determine the product branching ratios. Calculations are underway to compare the reaction probabilities on the singlet and triplet surfaces. These are classical calculations that do not include the influence of the intersection seam. In subsequent calculations the coupling between the triplet and singlet states will be evaluated, and the dynamics investigated using surface hopping trajectory methods.

Figure 9: CASSCF(12e/10o)/D95+d Potential Energy Surface

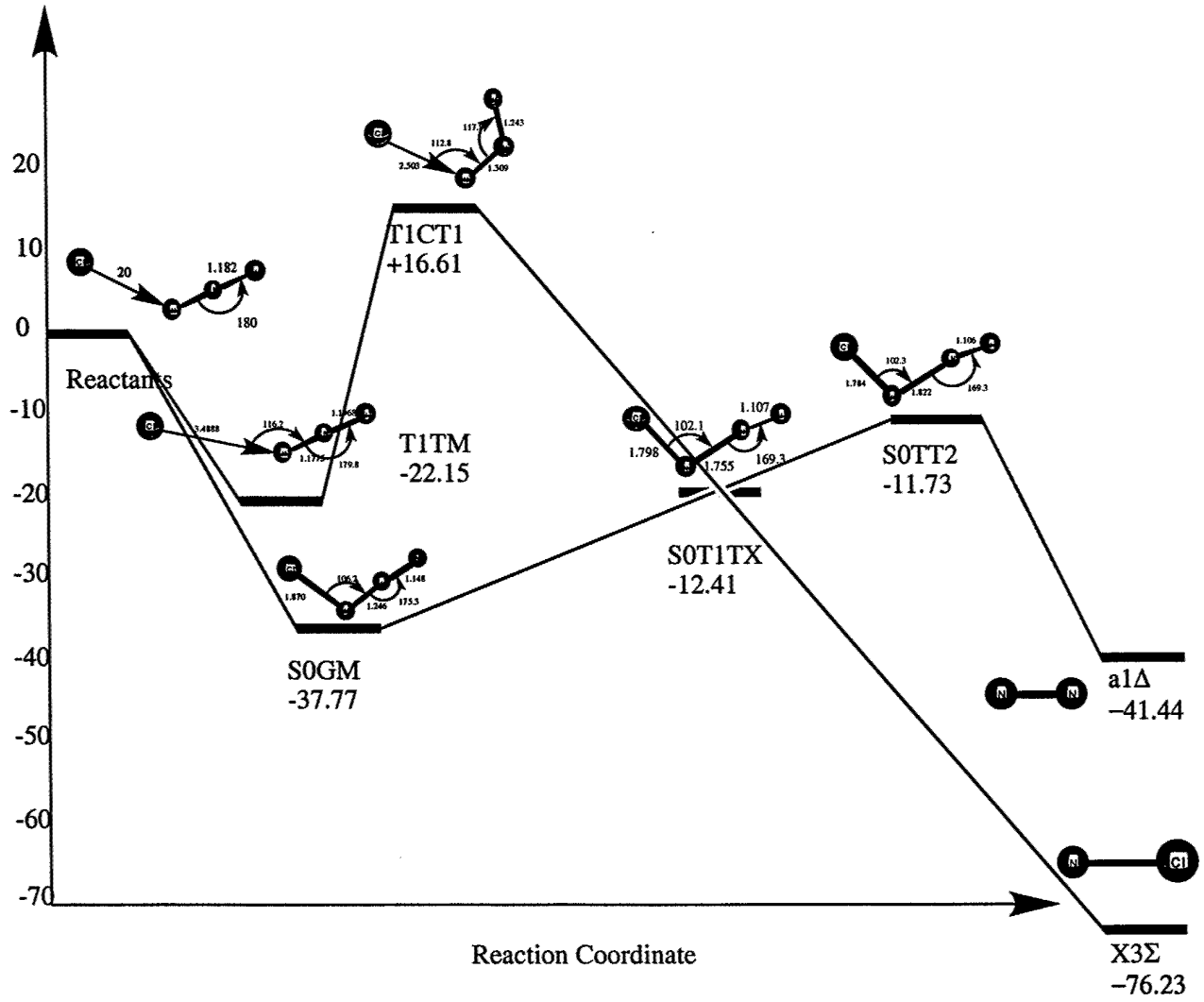

6. Measurement of the rate constants for $H+F_2$ and $H+Cl_2$

Investigation of the rate constants for $H+F_2$ and $H+Cl_2$ was initiated by Dr. G. Manke II. (AFRL/DELC). After performing an extensive review of the kinetic data for the HF chemical laser, Dr. Manke found that the uncertainty associated with the rate constant for the reaction $H+F_2 \rightarrow HF+F$ was unacceptably large (models of the laser system are strongly dependent on this parameter). As the facilities at Emory are better suited than those at AFRL/DELC for measurements of this kind, we have collaborated on new studies of H atom kinetics. The $H+Cl_2$ reaction was investigated as a means of testing the techniques used for these measurements. In addition we wanted to reduce the considerable uncertainty associated with the rate constant for this reaction (the reported values range from 0.39×10^{-11} to 3.5×10^{-11} cm^3 s^{-1}).

A time-resolved photolysis – probe technique is being used to follow H atom kinetics. H atoms are produced by pulsed laser photolysis of H_2S. The atoms are detected using two-photon excitation of the 2^2S-1^2S transition at 243.2 nm. Collisions convert 2^2S to 2^2P, and the subsequent Lyman α emission at 121.6 nm is detected by a solar blind photomultiplier (Hamamatsu R6835). A narrow band interference filter (Acton 122-N-1D) is used to block scattered light from the photolysis and probe lasers. The decay of the H atom concentration is followed by varying the delay between the photolysis and probe pulses.

Mixtures of H_2S/F_2 or H_2S/Cl_2 flowed slowly through the photolysis cell. The primary carrier gas used in these experiments was Ar. To ensure that the measurements were made under pseudo first order conditions the H_2S pressure was kept below 0.02 Torr. F_2 or Cl_2 partial pressures were in the 0.1 to 0.3 Torr range. Ar buffer gas was added to bring the total pressure in the cell to around 100 Torr. This was done to effect translational cooling of the H atoms prior to reaction and to limit diffusion. Translational relaxation of the H atoms was verified by examining the excitation profile of the 2^2S-1^2S transition. The Doppler profile of this line was consistent with a translational temperature of 300 K.

Kinetic runs were made with the probe laser tuned to the center of the excitation line. Fig. 10 shows a comparison of the H atom decay following photolysis Ar/H_2S and $Ar/H_2S/Cl_2$ mixtures. Rapid removal of H by the reaction with Cl_2 is easily observed by this technique. A plot of the H atom decay rate vs. $[Cl_2]$ yielded a rate constant of $(2.8 \pm 0.3) \times 10^{-11}$ cm^3 s^{-1}. This value is within the reported range and supports measurements that yielded relatively large rate constants.

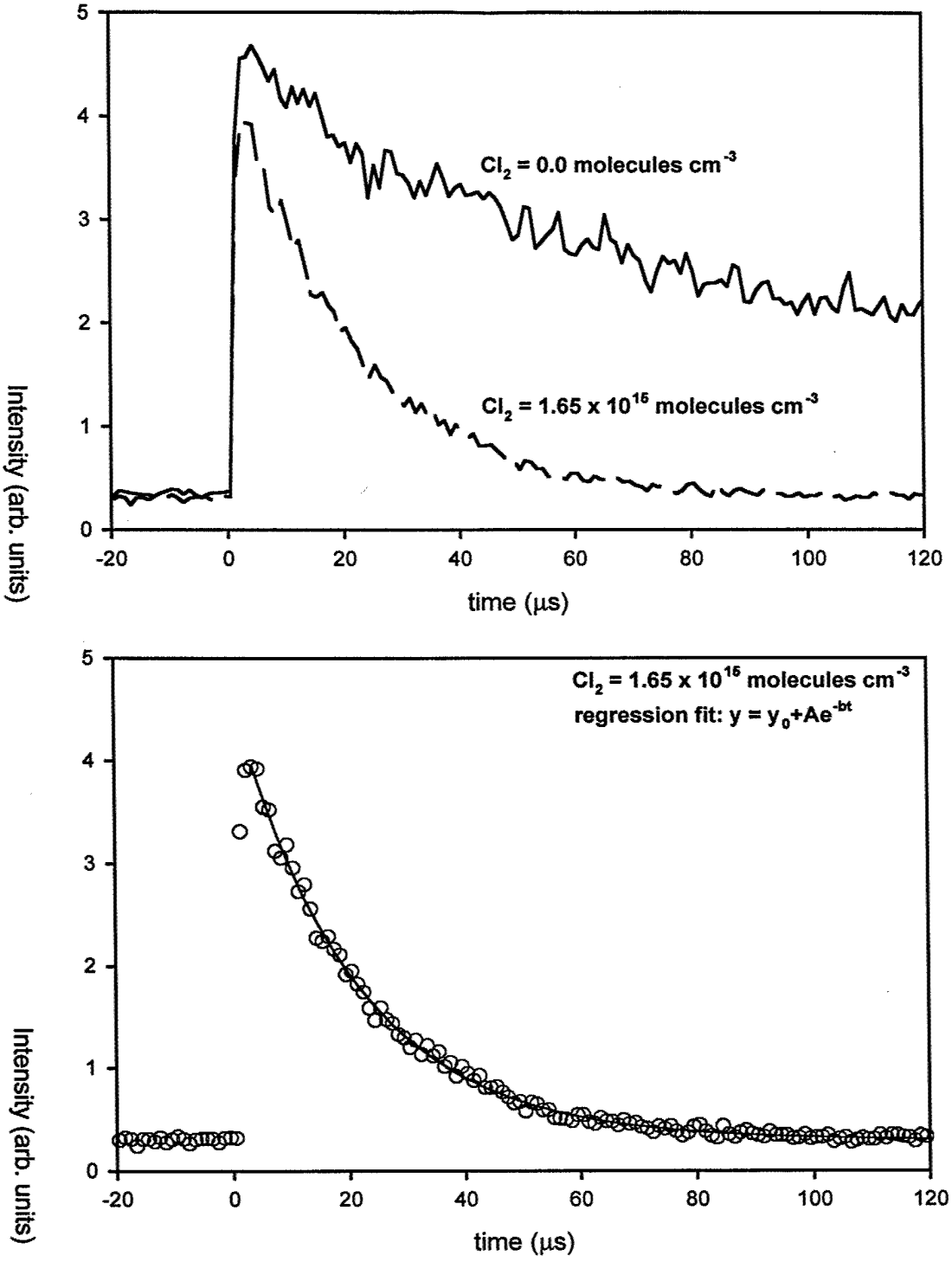

Figure 10. Representative H + Cl_2 data is shown. The slow decay in the absence of Cl_2 in the upper panel is attributed to diffusion and H atom loss via reaction with H_2S. The lower panel demonstrates the quality of the fit to a single exponential decay. The corresponding rate constant is 2.97 ± 0.04 cm^3 $molecules^{-1}$ s^{-1}.

Attempts to characterize the $H+F_2$ reaction by this approach were less successful. There were indications that some of the problems may stem from a pre-reaction between H_2S and F_2. Previous studies report that this reaction is very slow, but adding F_2 to the photolysis cell dramatically reduced the signal from prompt H atoms (the signal seen at the minimum photolysis-probe delay time). The temporal profile of H atoms in the presence of F_2 exhibited multi-exponential decay characteristics. The reaction of H with F_2 produces vibrationally excited HF, and we considered the possibility that multi-exponential decay was a consequence of the sequence

$$H + F_2 \rightarrow HF(v) + F$$

$$HF(v) + h\nu(243\ nm) \rightarrow H + F$$

$$H + 2h\nu(243) \rightarrow H^*$$

but models based on this scheme were unable to reproduce the complete family of decay curves. We also considered the possibility that a product from the pre-reaction was complicating the kinetics through secondary photochemical reactions. To test this notion we are experimenting with ways to minimize the time between mixing the reactants and photo-initiating the reaction. We have added a pulsed valve to the photolysis cell so that the H_2S can be introduced in brief busts, and the reaction initiated within a few milliseconds after mixing. Measurements with this system are currently in progress.

Publications

1. A. V. Kommisarov, V. Goncharov, and M. C. Heaven, in XIII International Symposium on Gas Flow and Chemical Lasers (SPIE, Florence, Italy).
   Proc. SPIE-Int. Soc. Opt. Eng, **4184,** 7 (2001)
   "Chemical Oxygen Iodine Laser Kinetics and Mechanisms"

2. M. C. Heaven, in Chemical Dynamics in Extreme Environments, Advanced Series in Physical Chemistry, Editor, R. A. Dressler, World Scientific, p138-205 (2001).
   "Chemical Dynamics in Chemical Laser Media"

3. A. V. Komissarov, G. C. Manke II, S. J. Davis and M. C. Heaven, *J. Phys. Chem.* In prepartion

   "Rate Constant for the Self-Annihilation of $NCl(a^1\Delta)$"

Ph. D. Thesis

Alexey L. Kaledin, Emory University, December 2000

"Spectroscopy and dynamics of small molecules in the gas phase: Application of theory"

Interactions

We have kept in contact with the group at AFRL/DELC who are working on the development of AGIL (Drs. Gordon Hager and Gerald Manke II). Our rate constants for NCl(a) quenching and self-annihilation are being used in their models of the sub-sonic AGIL device, and in the design of a super-sonic device. The computational modeling group at Logicon RDA has identified key reactions in the AGIL system for which temperature dependent rate constant and product branching ratio data are needed. Where possible, we are adapting our research program to obtain these data. We remain focused on the chemical kinetic and dynamics issues, to ensure that our work has intrinsic fundamental value consistent with the aims of the Molecular Dynamics program.

As noted above, the kinetic studies of $H+Cl_2$ and $H+F_2$ developed from conversations with the group at AFRL/DELC. Dr. Manke visited our laboratory for the week of Sept. 15-21 to participate in these experiments. We are currently preparing a manuscript that describes the $H+Cl_2$ results.

The P.I. participated in a one-day workshop on the AGIL project at Logicon RDA (NM) on July 23.

Studies of ro-vibrational energy transfer between the levels of CO(X) are being carried out at AFRL. This project provides data that may be used to interpret and model the behavior of CO overtone lasers. Capt. Stephen Phipps made an extensive study of CO(v,J)+CO collisions using IR pump probe techniques. As both the excitation and probe lasers had sub-Doppler linewidths, the data also revealed interesting facets of the competition between translational and rotational relaxation in this system. Capt. Phipps was registered with the University of New Mexico (UNM) as a Ph. D. student, and the CO work formed the core of his graduate research. Interpretation of the energy transfer data was not straightforward, and Capt. Phipps advisors at UNM are not experts in this field. At the request of Dr. Gordon Hager I participated in the interpretation of the data, and traveled to

AFRL on June 8 for this purpose. I then agreed to be a member of the examining committee for Capt. Phipps Ph. D. defense. I returned to UNM on Sept. 17 to attend the thesis defense, which was successful. I am continuing my involvement in this project, and we are currently preparing a manuscript that describes the key findings of Dr. Phipps work.

We are collaborating with Dr. S. J. Davis (Physical Sciences Inc.) on the development of a diode laser based diagnostic tool for characterization of NCl(X) in AGIL systems. Our most recent contribution to this project has been calculation of absolute linestrengths for selected lines of the b-X 0-0 band. These data can be used to convert quantitative integrated absorption measurements to absolute concentrations. The results of our calculations were communicated to PSI in July.